Geochemistry Geophysics Geosystems G3
AN ELECTRONIC JOURNAL OF THE EARTH SCIENCES
Published by AGU and the Geochemical Society

Research Letter
Volume 6, Number 1
20 January 2005
Q01J15, doi:10.1029/2004GC000791
ISSN: 1525-2027

Enrichment of HFSE in chlorite-harzburgite produced by high-pressure dehydration of antigorite-serpentinite: Implications for subduction magmatism

Carlos J. Garrido
Departamento de Mineralogía y Petrología, Facultad de Ciencias, Universidad de Granada, 18002 Granada, Spain (carlosg@ugr.es)

Vicente López Sánchez-Vizcaíno
Departamento de Geología, Escuela Universitaria Politécnica, Universidad de Jaén, Linares, Jaén, Spain

María Teresa Gómez-Pugnaire
Departamento de Mineralogía y Petrología, Facultad de Ciencias, Universidad de Granada, 18002 Granada, Spain

Volkmar Trommsdorff
Institut für Mineralogie und Petrographie, ETH Zentrum, 8092 Zurich, Switzerland

Olivier Alard
Radiogenic Isotopic Group, Department of Earth Sciences, Walton Hall, Open University, Milton Keynes, MK7 6AA, UK

Jean-Louis Bodinier and Marguerite Godard
Laboratoire de Tectonophysique, ISTEEM, Université de Montpellier 2, Montpellier, France

[1] Depletion of high-field-strength trace elements (HFSE) relative to normal mid-ocean basalts (N-MORB) is the most distinctive geochemical fingerprint of subduction magmatism. Proposed hypotheses advocate that this "subduction" signature is acquired during melting and/or fluid transfer either in the mantle wedge or in the crust of the subducting oceanic plate. Here we provide field-based and geochemical evidence showing that high-pressure dehydration of antigorite-serpentinite produces chlorite-harzburgite relatively enriched in HFSE due to the stabilization of F-OH-Ti-clinohumite intergrowths with prograde olivine. Available experimental data indicate that in hydrated, intermediate to warm subduction zones, clinohumite-olivine intergrowths can be stable in prograde chlorite-harzburgite olivine at subarc depths. In these settings, deserpentinization may act as a source of fluids leaching large-ion lithophile elements (LILE), Pb, and Sr from the overlying crust and sediments on their way up to the mantle wedge. Stabilization of chlorite-harzburgites with clinohumite-olivine intergrowths in the mantle wedge, on the other hand, acts as a sink of HFSE by selectively fractionating them from other incompatible trace elements in fluids emanating from the slab. Resulting arc fluids in equilibrium with wedge chlorite-harzburgite are strongly depleted in HFSE and transfer this depletion to the overlying hot mantle wedge, where subduction magmas are generated.

Components: 7466 words, 6 figures, 3 tables.

Keywords: subduction magmatism; geochemistry; high-field-strength elements; antigorite serpentinite; chlorite-harzburgite; subduction fluids.

Index Terms: 3613 Mineralogy and Petrology: Subduction zone processes (1031, 3060, 8170, 8413); 1031 Geochemistry: Subduction zone processes (3060, 3613, 8170, 8413); 1037 Geochemistry: Magma genesis and partial melting (3619).

Received 2 July 2004; **Revised** 29 October 2004; **Accepted** 19 November 2004; **Published** 20 January 2005.

Garrido, C. J., V. López Sánchez-Vizcaíno, M. T. Gómez-Pugnaire, V. Trommsdorff, O. Alard, J.-L. Bodinier, and M. Godard (2005), Enrichment of HFSE in chlorite-harzburgite produced by high-pressure dehydration of antigorite-serpentinite: Implications for subduction magmatism, *Geochem. Geophys. Geosyst.*, *6*, Q01J15, doi:10.1029/2004GC000791.

Theme: Trench to Subarc: Diagenetic and Metamorphic Mass Flux in Subduction Zones
Guest Editors: Gray Bebout, Jonathan Martin, and Tim Elliott

1. Introduction

[2] Trace element abundances of most mid-ocean ridge and oceanic island basalts display smooth patterns when they are normalized to an appropriate composition and plotted in decreasing order of compatibility for the melt. Lavas erupted at subduction zones are a remarkable exception [*Kelemen et al.*, 2003a; *Tatsumi and Eggins*, 1995]. Subduction-related volcanic rocks commonly display patterns characterized by depletion of high-field-strength elements (HFSE: Nb, Ta, Zr, Hf, and Ti) relative to large-ion lithophile elements (LILE: e.g., Rb, Ba). The origin of this geochemical signature remains highly debated, and proposed hypotheses differ in the mechanisms and depth where it is generated [*Tatsumi and Eggins*, 1995]. "Mantle wedge" hypotheses link HFSE anomalies to the presence of Ti-rich minerals that retain these elements during melt generation and/or transport [*Kelemen et al.*, 1990] in the mantle above the downgoing slab. "Slab" hypotheses contend that HFSE depletions are due to processes related to the generation of fluids or melts distilled from the subducting plate. HFSE depletions are produced because LILE are more readily partitioned into H_2O-rich fluids/melts released by devolatilization or partial melting of slab rocks. Fluids released from the slab transfer this depletion to the overlying mantle wedge and trigger flux-melting of peridotite leading to arc volcanism [*Kelemen et al.*, 2003a; *Tatsumi and Eggins*, 1995, and references therein].

[3] In hydrated subduction zones, antigorite-serpentinite may occur in large portions of the mantle wedge [*Hyndman and Peacock*, 2003] and the incoming slab [*Ranero et al.*, 2003]. Experimental and theoretical work have shown that high-pressure dehydration of antigorite ($\approx Mg_{48}Si_{34}O_{85}(OH)_{62}$) serpentinites is a fertile source of H_2O-rich fluids at subarc depths [*Schmidt and Poli*, 1998; *Ulmer and Trommsdorff*, 1995]. There is increasing evidence showing that serpentinite subduction may also be a suitable source, among other elements, of Cl, B, Be, Sr and Li for arc volcanism [*Scambelluri et al.*, 1997, 2004a, 2004b; *Straub and Layne*, 2003a, 2003b]. Here we present geochemical and petrological evidence indicating that prograde chlorite-harzburgite produced by high-pressure dehydration of antigorite-serpentinite [e.g., *Hacker et al.*, 2003b; *Ulmer and Trommsdorff*, 1995] can partition effectively HFSE due to stabilization of intergrowths of F-OH-Ti-clinohumite in chlorite-harzburgite olivine. Combined with available experimental data, we propose that stabilization of such intergrowths in prograde chlorite-harzburgite olivine, coeval with deserpentinization, may be an alternative and concomitant origin of HFSE depletion of subduction fluids in some subduction settings.

2. Geological Setting

[4] In this paper we explore the behavior of HFSE during high-pressure dehydration of antigorite-serpentinite (atg-serpentinite) through the study of whole rock and mineral trace elements in samples from the Cerro del Almirez ultramafic complex (Betic Cordillera, S. Spain) (Figure 1a). The Almirez ultramafic massif preserves the only known field example of high-pressure breakdown of atg-serpentinite to chlorite-harzburgite (chl-harzburgite) [*Trommsdorff et al.*, 1998]. The ultramafic rocks of Cerro del Almirez form three major bodies that are part of a thrust sheet (~400 m thick) covering an area of 3 km^2 (Figure 1a). The Almirez ultramafic rocks are interlayered with metapelites, marbles and graphite-bearing schists of the Nevado-Filábride metamorphic complex (Figure 1a), which is the uppermost complex in the internal zones of the Betic Cordillera.

[5] The mineral assemblage of Cerro del Almirez atg-serpentinite is similar to that of many atg-serpentinites in the Penninic zone of the Alps [*Trommsdorff et al.*, 1998, and references therein]. Almirez atg-serpentinite represents an early stage of prograde Alpine subduction zone metamorphism overprinting previously hydrated oceanic mantle [*Gómez-Pugnaire et al.*, 2000; *Puga et al.*, 1999]. High-pressure breakdown of atg-serpentinite

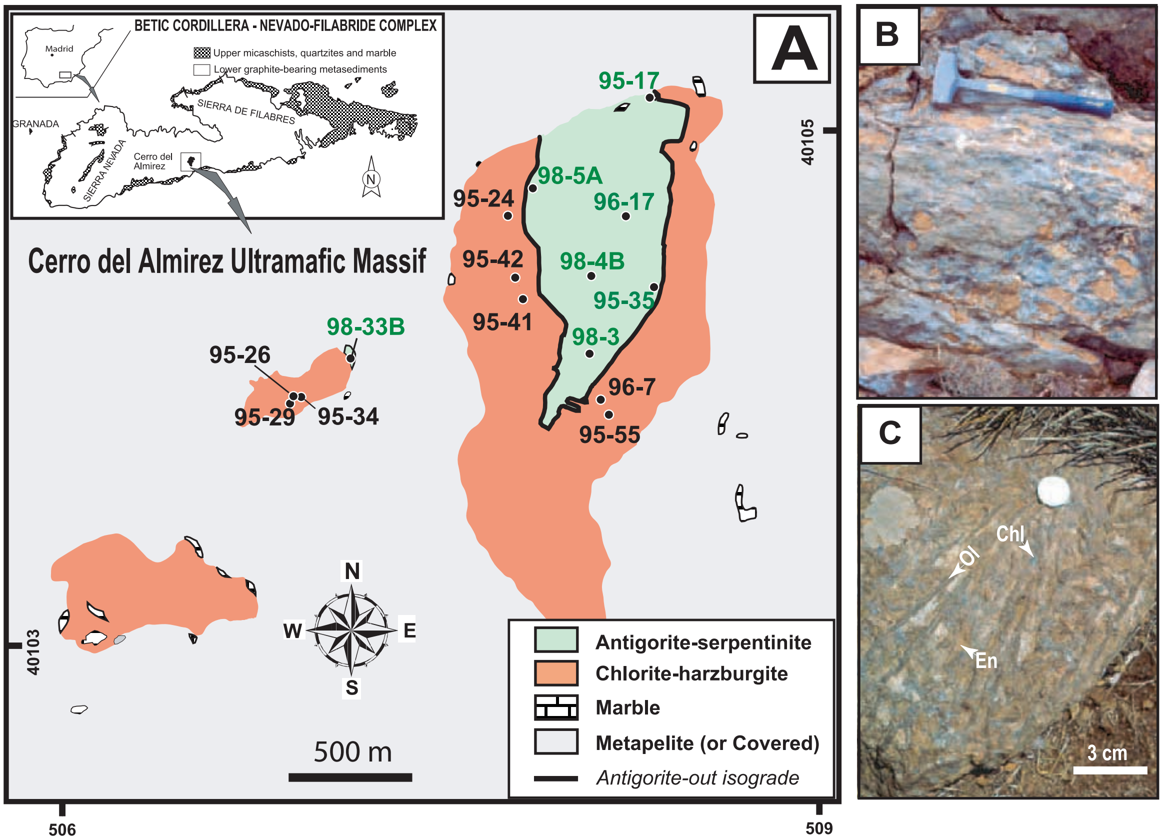

Figure 1. (a) Simplified geological map of the Cerro del Almirez massif showing the sample location of antigorite-serpentinite (green labels) and chlorite-harzburgite (black labels) (modified from *Schönbächler* [1999] and *Hürlimann* [1999]). Also shown in the map is the antigorite-out isograd. Inset: Geological sketch of the Nevado-Filábride metamorphic complex located in the internal zones of the western Betic Cordillera (S. Spain). Also shown is the location of the Cerro del Almirez massif within this complex. (b) Field photograph of a slightly foliated antigorite-serpentinite outcrop from the Almirez massif. (c) Field photograph illustrating the structure of a typical Almirez chlorite-harzburgite characterized by several centimeter long, spinifex-like brown olivine (Ol) immersed in a matrix of enstatite (En), chlorite (Chl), olivine, and minor tremolite.

occurred in a later stage during further subduction of atg-serpentinite [*López Sánchez-Vizcaíno et al.*, 2001; *Puga et al.*, 1999]. Petrographic evidence and thermodynamic calculations show that Almirez atg-serpentinite dehydrated directly to chl-harzburgite through the model reaction: antigorite = enstatite + olivine + chlorite + H_2O at 650 °C and pressures exceeding 1.7 GPa (>60 km) [*López Sánchez-Vizcaíno et al.*, 2001; *Trommsdorff et al.*, 1998]. This reaction, which we refer here to as "deserpentinization", may release as much as 12 wt% of H_2O and is presently regarded as an additional source of subarc fluids in subduction zones [*Ulmer and Trommsdorff*, 1995]. In Almirez, the stability of chlorite beyond the antigorite breakdown reaction limited the release of H_2O to about 6–7 wt% [*Scambelluri et al.*, 2004a; *Trommsdorff et al.*, 1998]. The contact between atg-serpentinite and chl-harzburgite crops out in Almirez as a tectonically undisturbed "deserpentinization front" interpreted as representing the "antigorite-out" isograd (Figure 1a) [*Trommsdorff et al.*, 1998]. Almirez atg-serpentinite is moderately foliated (Figure 1b) and its usual mineral assemblage is antigorite with minor olivine, diopside, chlorite, magnetite and rare tremolite. Almirez chl-harzburgite is massive and characterized by spinifex-like, arborescent olivine (Figure 1c) and elongated radiating enstatite in a matrix of chlorite, tremolite and magnetite. Olivine is either brown due to inclusions of magnetite, Fe-chromite and ilmenite [*Ruiz Cruz et al.*, 1999] or, less commonly, clear and lacking inclusions.

3. Sampling and Analytical Procedures

[6] For this study we selected 8 samples of chl-harzburgite and 7 of atg-serpentinite. Sample location is shown in Figure 1a. Most samples come from the main ultramafic body of the Almirez

Geochemistry Geophysics Geosystems G3 10.1029/2004GC000791

Table 1. XRF and ICP-MS Whole Rock Analyses of Almirez Antigorite-Serpentinite and Chlorite-Harzburgite[a]

	Antigorite-Serpentinite Samples							Chlorite-Harzburgite Samples								UB-(n)		
	AL95-17	AL95-35	AL96-17	AL98-03	AL98-04B	AL98-05A	AL98-33B	AL95-24	AL95-26	AL95-29	AL95-41	AL95-42	AL95-55	AL96-07	AL95-34	This Study	2σ	GSNL
SiO_2, wt%	40.19	41.78	40.68	40.08	39.33	40.25	40.97	42.13	40.79	43.96	43.02	42.89	42.73	44.02	45.58			
TiO_2	0.05	0.11	0.05	0.12	0.73	0.12	0.08	0.12	0.11	0.05	0.05	0.08	0.06	0.10	0.07			
Al_2O_3	2.40	3.35	2.27	2.70	3.29	2.81	2.42	3.11	1.65	1.63	2.56	2.96	3.06	3.30	2.65			
Fe_2O_3	7.42	7.30	8.50	8.51	8.34	8.04	7.82	7.75	8.28	8.97	7.92	8.47	8.54	8.40	7.87			
MnO	0.11	0.10	0.14	0.10	0.14	0.10	0.12	0.09	0.12	0.12	0.11	0.14	0.14	0.14	0.11			
MgO	37.29	33.98	36.71	37.70	37.58	38.18	36.04	38.57	42.57	41.34	41.64	41.08	40.67	40.02	40.07			
CaO	2.28	4.83	3.11	0.03	0.28	0.11	3.26	0.17	0.18	0.07	0.06	0.10	0.10	0.31	0.09			
Na_2O	*b.d.l.*	*b.d.l.*	*b.d.l.*	*b.d.l.*	*b.d.l.*	*b.d.l.*	*b.d.l.*	b.d.l.	*b.d.l.*	*b.d.l.*	*b.d.l.*	*b.d.l.*	*b.d.l.*	*b.d.l.*	*b.d.l.*			
K_2O	*b.d.l.*	*b.d.l.*	*b.d.l.*	*b.d.l.*	*b.d.l.*	*b.d.l.*	*b.d.l.*	b.d.l.	*b.d.l.*	*b.d.l.*	*b.d.l.*	*b.d.l.*	*b.d.l.*	*b.d.l.*	*b.d.l.*			
P_2O_5	0.01	0.01	0.01	0.02	0.04	0.01	0.01	0.12	0.04	0.02	0.02	0.01	0.03	0.02	0.05			
L.O.I.	10.37	8.96	8.87	11.62	11.35	11.38	9.72	8.61	4.62	2.66	4.18	4.49	5.17	3.09	3.70			
Total	100.1	100.4	100.3	100.9	101.1	101.0	100.4	100.7	98.36	98.83	99.56	100.2	100.5	99.40	100.2			
Rb, ppm	0.150	0.068	0.151	0.144	0.055	0.059	0.066	0.183	0.086	0.112	0.078	0.063	0.091	0.054	0.225	3.4	*0.2*	4
Sr	1.84	3.47	2.83	0.70	0.51	0.66	1.92	11	6	6	1.58	2.18	4.59	2.13	8	7.5	*0.6*	9
Y	2.20	2.10	2.21	0.96	1.27	1.48	2.85	1.91	0.60	0.68	0.87	0.99	0.77	0.82	0.57	2.23	*0.2*	2.50
Zr	0.36	0.33	0.28	0.58	0.35	0.31	0.21	2.57	3.88	0.26	0.34	0.28	0.38	0.48	0.55	3.55	*0.32*	4.00
Nb	0.16	0.11	0.08	0.11	0.29	0.30	0.20	2.87	8.91	1.00	0.24	0.23	1.13	1.62	2.76	0.048	*0.0044*	0.050
Cs	0.066	0.093	0.064	0.136	0.059	0.060	0.046	0.096	0.196	0.104	0.018	0.035	0.047	0.026	0.141	11.360	*0.368*	10.000
Ba	0.94	1.58	1.56	1.19	1.89	1.29	1.47	2.26	1.86	1.98	0.67	1.17	1.06	1.27	2.10	28.05	*0.56*	27.00
La	0.295	0.344	0.306	0.324	0.193	0.208	0.322	0.107	0.177	0.055	0.110	0.094	0.130	0.225	0.079	0.321	*0.008*	0.350
Ce	0.756	0.682	0.701	0.906	0.611	0.691	0.902	0.313	0.204	0.132	0.260	0.221	0.331	0.555	0.175	0.819	*0.017*	0.800
Pr	0.100	0.074	0.092	0.118	0.085	0.102	0.140	0.0473	0.0291	0.0164	0.0334	0.0283	0.0427	0.071	0.0210	0.116	*0.0012*	0.120
Nd	0.479	0.280	0.459	0.56	0.431	0.53	0.74	0.253	0.152	0.074	0.161	0.132	0.193	0.312	0.091	0.62	*0.0073*	0.60
Sm	0.146	0.094	0.174	0.134	0.120	0.159	0.230	0.086	0.0487	0.0204	0.0448	0.0392	0.0490	0.076	0.0242	0.216	*0.0061*	0.200
Eu	0.059	0.061	0.073	0.0400	0.0331	0.0437	0.068	0.0188	0.0144	0.0056	0.0106	0.0102	0.0088	0.0181	0.0079	0.084	*0.0033*	0.080
Gd	0.251	0.199	0.285	0.171	0.172	0.229	0.357	0.145	0.073	0.0289	0.064	0.065	0.066	0.094	0.0309	0.337	*0.0087*	0.300
Tb	0.0487	0.0435	0.056	0.0260	0.0308	0.0418	0.067	0.0298	0.0134	0.0065	0.0128	0.0150	0.0126	0.0176	0.0065	0.063	*0.0012*	0.060
Dy	0.378	0.366	0.427	0.178	0.231	0.297	0.494	0.254	0.102	0.067	0.114	0.137	0.110	0.134	0.062	0.461	*0.0153*	0.380
Ho	0.085	0.088	0.093	0.0387	0.054	0.066	0.107	0.069	0.0236	0.0231	0.0349	0.0399	0.0303	0.0327	0.0203	0.102	*0.0023*	0.090
Er	0.256	0.288	0.289	0.118	0.184	0.212	0.314	0.256	0.075	0.129	0.173	0.161	0.141	0.120	0.102	0.303	*0.0082*	0.280
Tm	0.0390	0.0468	0.0439	0.0191	0.0310	0.0336	0.0471	0.0457	0.0128	0.0329	0.0398	0.0356	0.0349	0.0258	0.0281	0.0457	*0.0004*	0.0450
Yb	0.259	0.315	0.277	0.140	0.224	0.233	0.303	0.328	0.092	0.289	0.317	0.291	0.328	0.228	0.281	0.304	*0.0034*	0.280
Lu	0.0432	0.055	0.0451	0.0266	0.0419	0.0408	0.0494	0.057	0.0171	0.053	0.058	0.052	0.067	0.0449	0.059	0.052	*0.0010*	0.0450
Hf	0.024	0.027	0.020	0.030	0.025	0.024	0.017	0.047	0.040	0.010	0.020	0.022	0.019	0.017	0.021	0.13	*0.004*	0.10
Ta	0.0087	0.0049	0.0037	0.0054	0.0212	0.0224	0.0107	0.238	0.90	0.0466	0.0128	0.0123	0.0260	0.072	0.183	0.0196	*0.0005*	0.0200
Pb	0.23	0.42	0.33	0.30	0.11	0.09	0.16	0.17	0.49	0.58	0.20	0.22	0.34	0.40	0.64	13.54	*0.88*	13.00
Th	0.079	0.0126	0.0208	0.088	0.052	0.0465	0.0237	0.163	0.55	0.095	0.078	0.0409	0.085	0.119	0.0498	0.066	*0.0059*	0.070
U	0.0324	0.0104	0.0118	0.0166	0.0139	0.0114	0.0151	0.052	0.0347	0.0283	0.058	0.072	0.094	0.158	0.0267	0.058	*0.0084*	0.070

[a] L.O.I., Loss On Ignition; b.d.l., below detection limit; GSNL, working values for UB-(n) [*Govindaraju*, 1994].

massif and were taken at both sides of the deserpentinization "isograd" (Figure 1a). All selected samples are homogeneous and lack veins. Large amount of each sample (>3 kg) were crushed and powders were made in an agate ring mill. Whole rock major and trace element data are given in Table 1. Whole rock major elements were analyzed in fused beads by XRF in a PHILIPS PW1404/10 instrument at the CIC (Universidad de Granada, Spain) using standard procedures. Whole rock trace element data were determined on a quadrupole VG-PlasmaQuad Inductively Coupled Plasma-Mass Spectrometer (ICP-MS) at ISTEEM (Université de Montpellier 2, France) following the procedure described by *Ionov et al.* [1992]. REE, U, Th, Sr, Zr, Hf, Rb and Ba concentrations were determined by external calibration. To avoid memory effects due to the intake of concentrated Nb-Ta solutions in the instrument, Nb and Ta concentrations were determined by using Zr and Hf, respectively, as internal standards. This technique is an implementation to ICP-MS analysis of the method described by *Jochum et al.* [1990] for the analysis of Nb by spark-source mass spectrometry. Detection limits obtained by long-term (several years) analyses of chemical blanks at ISTEEM are given by *Ionov et al.* [1992] and *Garrido et al.* [2000]. The composition of reference sample UB-(n), analyzed as an unknown during the same analytical runs as Almirez samples (Table 1), shows an excellent agreement with working values for this sample [*Govindaraju*, 1994] (GSNL in Table 1). The long-term analytical reproducibility of ICP-MS analyses at ISTEEM for UB-N is between 13–20% for Nb, Ta and U and less than 10% for the rest of the trace elements [*Garrido et al.*, 2000]. For lower concentrations, the long-term reproducibility of the international reference sample PCC-1 (dunite) is between 2–15% for all elements but Ta (19%) [*Godard et al.*, 2000].

[7] Trace element analyses of minerals of chl-harzburgite sample AL95-07 are given in Table 2. Also in this table we report the composition of F-OH-Ti clinohumite intergrowths in olivine of chl-harzburgite sample AL95-34. Mineral trace element data were obtained in sample thick sections by Laser Ablation-ICP-MS (LA-ICP-MS) at The Open University (UK) using a frequency quintupled Nd:YAG UV (213 nm) laser system (UP213, Merchanteck-New Wave Research) linked to an HP7500a ICP-MS. Ablation was performed in pure He-atmosphere (0.65 ± 0.01 l min^{-1}) mixed before entering the torch with a flow of Ar ($\sim$1.00 $\pm$ 0.05 l min^{-1}). The ICP-MS was operated with its shield torch at 1400 W and tuned to produce maximum sensitivity for the medium and high masses while keeping the oxide production rate low ($^{248}ThO/^{232}Th \leq 1\%$). Typical spot sizes were between 60 and 80 μm, energy beam of ~0.5 mJ yielding an energy density about 10 J cm^{-2}, and a repetition pulse rate set at 10Hz. Data reduction was carried out using the GLITTER software [*Van Achtebergh et al.*, 2001]. SiO_2 content of minerals, obtained by electron microprobe, was used as internal standard. The NIST612 glass [*Pearce et al.*, 1997] was used as an external standard. This double standardization allows correction for variations in ablation yield and instrumental drift [*Longerich et al.*, 1996]. Data in Table 2 are averages of "*n*" analyses of different mineral grains from the same sample. Errors represent ±1 the standard deviation of the *n* analyses (i.e., external error). The accuracy and precision of our LA-ICP-MS analyses can be assessed by comparing repeated measurements of standard GOR128 glass (Table 2) with published values for this standard obtained in several laboratories using various analytical techniques [*Jochum et al.*, 2000] (Table 2). No mineral standards of international validity are commercially available for LA-ICP-MS yet. Our LA-ICP-MS trace element results in PH-1 clinopyroxene (a peridotite from the French Massif Central peridotite) [*Alard et al.*, 1996] (Auxiliary Material Table 1[1]) are in good agreement with values obtained in several laboratories using both solution and LA-ICP-MS [*Downes et al.*, 2003]. Differences between solution and LA-ICP-MS analyses for the most incompatible elements (i.e., LILE and LREE) (Auxiliary Material Table 1) are due to the presence of fluid and melt inclusions in separates of clinopyroxene [*Garrido et al.*, 2000].

4. Geochemistry of Chlorite-Harzburgite

[8] Figure 2a shows the patterns of the trace element abundances of chl-harzburgites normalized to that of average Almirez atg-serpentinite. Normalized patterns of chl-harzburgite display marked positive spikes of Nb, Ta, Zr and Hf indicating that they strongly fractionated HFSE relative to light (LREE) and middle (MREE) rare earth elements. Chl-harzburgites show statistically significantly higher Nb/La, Ta/La, Zr/Sm and Hf/Sm ratios than precursor atg-serpentinites (Table 3). This indicates

[1]Auxiliary material is available at ftp://ftp.agu.org/apend/gc/2004GC000791.

Table 2. Trace Element Composition of Almirez Chl-Harzburgite Minerals Analyzed by LA-ICP-MS[a]

	Chlorite-Harzburgite AL95-07										AL95-34 (chl-hz)		MPI-Glass GOR 128			
	Clear Olivine		Brown Olivine		Tremolite		Chlorite		Enstatite		F-OH-Ti-Clinohumite Intergrowths		This Study		*Jochum et al.* [2000]	
Mineral	Avg(n = 3)	± *1*σ	Avg(n = 3)	± *1*σ	Avg(n = 4)	± *1*σ	Avg(n = 5)	± *1*σ	Avg(n = 4)	± *1*σ	Avg(n = 4)	± *1*σ	Avg(n = 10)	± *1*σ	RV	±1σ
Ti, ppm	31	*±11*	433	*±183*	121	*±46*	112	*±12*	144	*±5*	9399	*±5895*	1852	*±154*	1680	*±20*
Rb	0.01	*±0.01*	0.010	*±0.002*	0.10	*±0.01*	0.05	*±0.01*	0.08	*±0.01*	0.09	*±0.02*	0.35	*±0.01*	0.39	*±0.01*
Sr	0.1	*±0.2*	0.31	*±0.07*	13	*±1*	0.24	*±0.08*	3.5	*±0.5*	8	*±2*	31.2	*±1.2*	31	*±1.00*
Zr	0.012	*±0.005*	0.805	*±0.06*	0.090	*±0.002*	0.16	*±0.02*	0.139	*±0.009*	1.0	*±0.1*	10.26	*±0.25*	10.2	*±0.20*
Nb	0.1	*±0.1*	3.1	*±0.6*	0.14	*±0.01*	0.19	*±0.03*	1.3	*±0.1*	75	*±7*	0.1094	*±0.006*	0.11	*±0.01*
Ba	0.01	*±0.01*	0.15	*±0.03*	0.44	*±0.05*	0.07	*±0.02*	1.2	*±0.2*	1.8	*±0.3*	1.04	*±0.03*	1.09	*±0.04*
La	0.002	*±0.003*	0.027	*±0.002*	0.17	*±0.01*	0.014	*±0.001*	0.35	*±0.01*	0.06	*±0.009*	0.124	*±0.006*	0.124	*±0.005*
Ce	0.002	*±0.002*	0.07	*±0.01*	0.80	*±0.03*	0.040	*±0.003*	0.88	*±0.07*	0.11	*±0.01*	0.42	*±0.01*	0.46	*±0.020*
Pr	0.0003	*±0.0001*	0.009	*±0.001*	0.200	*±0.003*	0.0044	*±0.0003*	0.096	*±0.005*	0.012	*±0.002*	0.101	*±0.005*	0.105	*±0.004*
Nd	0.0014	*±0.0005*	0.035	*±0.006*	1.42	*±0.05*	0.017	*±0.001*	0.41	*±0.01*	0.039	*±0.008*	0.82	*±0.02*	0.78	*±0.02*
Sm	0.0006	*±0.0001*	0.007	*±0.002*	0.71	*±0.04*	0.0046	*±0.0003*	0.099	*±0.004*	<0.01		0.56	*±0.02*	0.54	*±0.02*
Eu	0.0004	*±0.0001*	0.0016	*±0.0005*	0.17	*±0.01*	0.0012	*±0.0001*	0.0205	*±0.0005*	0.004	*±0.001*	0.27	*±0.01*	0.27	*±0.01*
Gd	0.0021	*±0.0002*	0.009	*±0.005*	1.02	*±0.08*	0.0037	*±0.0004*	0.13	*±0.01*	0.019	*±0.005*	1.23	*±0.05*	1.21	*±0.04*
Dy	0.004	*±0.001*	0.08	*±0.01*	1.60	*±0.10*	0.005	*±0.001*	0.20	*±0.01*	0.038	*±0.002*	2.12	*±0.07*	1.97	*±0.05*
Ho	0.0033	*±0.0005*	0.042	*±0.001*	0.35	*±0.02*	0.0012	*±0.0001*	0.051	*±0.002*	0.017	*±0.002*	0.48	*±0.02*	0.44	*±0.01*
Er	0.026	*±0.003*	0.33	*±0.01*	1.20	*±0.06*	0.0050	*±0.0003*	0.199	*±0.008*	0.09	*±0.01*	1.46	*±0.04*	1.40	*±0.06*
Tm	0.0102	*±0.0004*	0.102	*±0.002*	0.22	*±0.01*	0.0015	*±0.0001*	0.042	*±0.002*	0.028	*±0.007*	0.22	*±0.01*	0.20	*±0.01*
Yb	0.137	*±0.006*	1.03	*±0.04*	1.6	*±0.1*	0.019	*±0.001*	0.36	*±0.02*	0.38	*±0.04*	1.50	*±0.05*	1.39	*±0.06*
Lu	0.036	*±0.002*	0.198	*±0.001*	0.20	*±0.01*	0.007	*±0.001*	0.066	*±0.004*	0.088	*±0.01*	0.221	*±0.008*	0.210	*±0.010*
Hf	0.0006	*±0.0002*	0.05	*±0.01*	0.013	*±0.001*	0.0023	*±0.0003*	0.0084	*±0.0006*	0.043	*±0.01*	0.358	*±0.012*	0.351	*±0.008*
Ta	0.003	*±0.002*	0.15	*±0.03*	0.008	*±0.001*	0.002	*±0.001*	0.082	*±0.005*	3.9	*±0.6*	0.020	*±0.001*	0.028	*±0.006*
Th	0.0005	*±0.0003*	0.0021	*±0.0003*	0.017	*±0.001*	0.004	*±0.001*	0.28	*±0.02*	0.026	*±0.004*	0.0080	*±0.0003*	0.007	*±0.001*
U	0.0008	*±0.0005*	0.018	*±0.004*	0.026	*±0.003*	0.015	*±0.002*	0.19	*±0.02*	0.12	*±0.02*	0.0114	*±0.0004*	0.013	*±0.010*

[a] MPI-Glass GOR128, reference sample of the Max-Plank Institute, glass GOR128; RV, recommended values of *Jochum et al.* [2000].

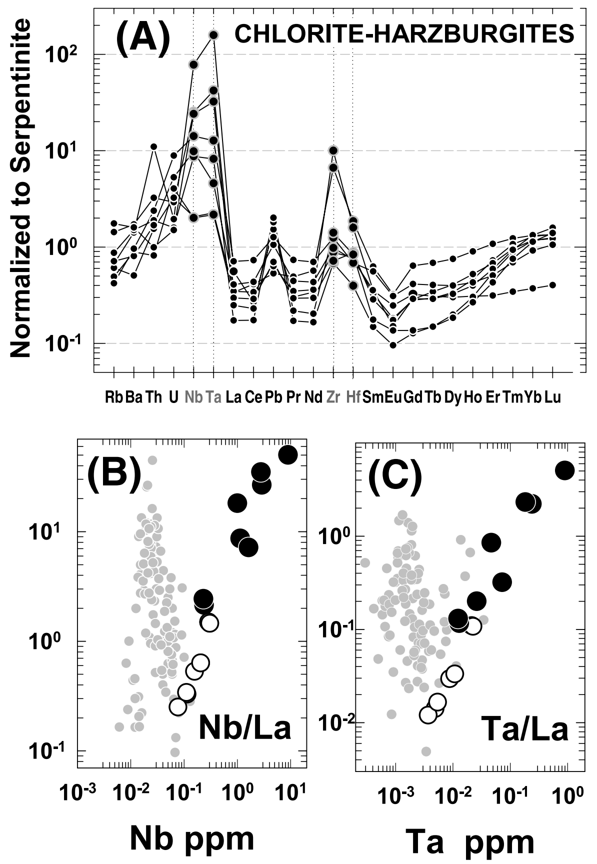

Figure 2. (a) Whole rock trace element abundances of Almirez chlorite-harzburgite samples normalized to the average trace element abundances of Almirez serpentinite. Light gray symbols are HFSE (Nb, Ta, Zr, and Hf). (b and c) Plots of Nb/La versus Nb and Ta/La versus Ta comparing Almirez chlorite-harzburgite and antigorite-serpentinite samples with a large geochemical database of oceanic peridotites (small gray circles) compiled by *Bodinier and Godard* [2003]. Outsized open and black symbols are Almirez antigorite-serpentinite and chlorite-harzburgite, respectively.

that fluids released during formation of prograde chl-harzburgites had complementary low Nb-Ta/LREE and Zr-Hf/MREE ratios. In agreement with experimental evidence [*Tatsumi et al.*, 1986], our data show that the Zr and HREE concentrations of most chl-harzburgites are similar to those of precursor atg-serpentinites, and these elements were hence effectively immobile during deserpentinization (Figure 2a). The high Zr/Sm and Hf/Sm ratios of chl-harzburgites are therefore due primarily to the preferential mobility of MREE into fluids. In contrast, relative gains of Nb, Ta, and U observed in chl-harzburgite require high fluid/rock ratios as well as preferential LREE partitioning into fluids, implying that formation of chl-harzburgite by dehydration occurred in an open system for these trace elements. The positive correlations of Nb/La with Nb, and Ta/La with Ta in Almirez samples (Figures 2b and 2c) indicates that dehydration of atg-serpentinite generated chl-harzburgite with high Nb/La and Ta/La ratios, and substantial Nb and Ta enrichments. To our knowledge, such Nb and Ta enrichments have not been previously reported in any oceanic peridotite (Figures 2b and 2c). Our data indicate that chl-harzburgite behaved as a sink of HFSE (notably Nb and Ta) during open-system dehydration of atg-serpentinite.

5. Origin of HFSE Enrichments in Chlorite-Harzburgite

[9] Figure 3a shows the result of trace element mass balance computations in chl-harzburgite sample AL95-07 combining mineral modal proportion with whole rock (Table 1) and mineral trace element data (Table 2). The mass balance indicates that the main carrier of HFSE in Almirez chl-harzburgite is brown olivine (Figure 3). Brown olivine accounts for >70 and >65 wt% of the chl-harzburgite budget of HFSE and most HREE, respectively (Figure 3a). The contribution of other chl-harzburgite minerals to the HFSE budget is minor or negligible (Figure 3a), and their normalized trace element patterns do not display positive HFSE anomalies relative to trace elements of similar compatibility (Figure 3c). Brown olivine strongly fractionates HFSE from trace elements of similar compatibility, resulting in normalized trace element patterns with positive anomalies of Nb-Ta and Zr-Hf (Figure 3b). Tremolite and enstatite display negative anomalies of Zr and Hf (Figure 3c) indicating they were equilibrated with a mineral having higher partitioning for HFSE. Clear olivine lacks any marked positive HFSE anomaly and its normalized pattern (Figure 3b) is similar to that of mantle peridotite olivine from ultramafic massifs and xenoliths [*Bedini and Bodinier*, 1999; *Garrido et al.*, 2000; *Sun and Kerrich*, 1995] (light gray field in Figure 3b). These results point to strong fractionation of HFSE and HREE into chl-harzburgite brown olivine, suggesting that the formation of this phase (or its precursor phase) during antigorite breakdown may have been the cause of the whole rock HFSE enrichment observed in Almirez chl-harzburgite (Figure 2).

[10] The dissimilar partitioning of HFSE between brown and clear olivines (Figure 3b) may suggest that fractionation of HFSE into brown olivine is due to trapping of Ti-Cr oxides during antigorite

Table 3. Statistics of Key Trace Element Ratios of Almirez Antigorite-Serpentinite and Chlorite-Harzburgite[a]

		Nb/La	Ta/La	Zr/Sm	Hf/Sm	Nb/Ta	Zr/Hf	Ba/La	Pb/Ce	Sr/Nd
Chl-harzburgite	Mean	18.8	1.40	21.7	0.55	20	35	15.8	1.81	38.3
(n = 8)	Median	13.4	0.58	10.4	0.52	19	26	11.5	1.02	31.1
	Std. Error	6.1	0.61	8.8	0.08	4	10	3.9	0.52	11.0
Atg-serpentinite	Mean	0.7	0.05	2.53	0.17	18	14	5.3	0.32	4.1
(n = 7)	Median	0.5	0.03	2.45	0.17	19	14	4.6	0.30	2.6
	Std. Error	0.2	0.02	0.44	0.03	1	1	0.8	0.07	1.5
				Comparison of Means						
T test	*p*	0.02	na	na	0.002	0.66	0.07	0.03	0.02	na
	Result	R	-	-	R	**FR**	**FR**	R	R	-
Mann-Witney U test	*p*	0.001	0.001	0.001	0.002	0.9	0.02	0.008	0.002	0.003
	Result	R	R	R	R	**FR**	R	R	R	R

[a] Reported descriptive statistics are the mean, median, and standard errors of "*n*" samples of each rock type. Also reported are two statistical tests comparing the trace element ratio of chl-harzburgite with those of atg-serpentine: T test: results of the T test for unequal and unknown variances; na, the T test is nonapplicable because the assumption of normality required by the T test is not fulfilled; Mann-Whitney U test: results of the nonparametric (i.e., no assumptions about the distribution of the underlying population) Mann-Whitney U test. In both tests the null hypothesis is "the two means are equal," and the level of significance is 5; p is the empirical significance test of a given test such as $p < 0.01$ indicates a confidence level greater than 0.99; R and FR stand for "reject" and "fail to reject" the null hypothesis, respectively. If rejected, it is likely that the two means are different (i.e., two populations) with a confidence level of p. All statistical computations were carried out using SPSS® (version 11) statistical software.

breakdown. TEM studies [*Ruiz Cruz et al.*, 1999] of Almirez brown olivines have demonstrated, however, that these oxides are exsolution products from precursor high-Ti "olivine". *Risold et al.* [2001] have shown that high Ti contents in "olivine" are due to humite type planar defects. Conversely to continuous solid solution mineral series, the humite mineral group [$n(Mg_2SiO_4)Mg(OH,F)_2$; n = 1, 2, 3 or 4] and olivine are stoichiometrically colinear with discrete compositions between the end-members olivine and norbergite forming a polysomatic mineral series [e.g., *Thompson*, 1978; *Veblen*, 1991]. Structurally, the members of the olivine-humite series may form parallel intergrowths that have been observed in olivine from different settings [*Kitamura et al.*, 1987; *Tilley*, 1951]. In Almirez chl-harzburgite sample AL95-34 we have identified optically relict intergrowths of F-Ti-OH clinohumite ($(M_8Si_4O_{16})M_{(1\text{-}x)}Ti_x(OH,F)_{(2\text{-}2x)}O_{2x}$, where M is Mg, Fe, Mn and Ni, and $x < 0.5$) within brown olivine (Figure 4). Clinohumite occurs as intergrowths (Figure 4b) and lamellae within brown olivine. Up to 0.5 atoms of Ti per formula unit can be substituted for MgH_2 in clinohumite making it a potential host for titanium in the upper mantle [*Scambelluri et al.*, 2001b; *Weiss*, 1997]. In Almirez brown olivine, we have measured by microprobe TiO_2 contents of up to 1.2 wt% which would correspond to a content of about 25 mol% of F-OH-Ti-clinohumite in precursor olivine (Figure 5). LA-ICP-MS analyses of F-OH-Ti-clinohumite intergrowth relics in sample AL95-34 have an average trace element normalized pattern with strong positive anomalies of Nb, Ta, Zr and Hf (Figure 3b; Table 2) and elevated HFSE contents [see also *Scambelluri et al.*, 2001b; *Ulmer and Trommsdorff*, 1999; *Weiss*, 1997] indicating that HFSE were hosted in clinohumite intergrowths within precursor "olivines". We emphasize that none of our chl-harzburgite samples contains veins of clinohumite, and hence the HFSE enrichments observed in harzburgite whole rocks are a primary signature of their constituting minerals (Figure 3). As identified texturally (Figure 4), F-OH-Ti clinohumite intergrowths within olivine have disappeared by breakdown in most chl-harzburgites, but some survived prograde metamorphism (e.g., sample AL95-34) due likely to the effect of fluorine in stabilizing F-OH-Ti-clinohumite at higher temperature for a given pressure (Figure 6a). Prograde dehydration and decompression of Almirez chl-harzburgite led to continuous breakdown of clinohumite intergrowths in olivine according to the reaction [*Evans and Trommsdorff*, 1983; *Trommsdorff and Evans*, 1980; *Weiss*, 1997] F-OH-Ti-clinohumite = olivine + ilmenite + fluid (H_2O, F) (Figure 6a), producing brown olivines (Figure 4b).

[11] The above petrological, mineralogical and trace element evidence points to the formation of high-Ti "olivine", owing to the stabilization of F-OH-Ti-clinohumite intergrowths (Figure 4), as the cause of the HFSE enrichment observed in Almirez chl-harzburgite (Figure 2). Our results suggest that outcoming fluids in equilibrium with chl-harzburgite must have been depleted in HFSE relative to LILE, LREE and MREE. *Scambelluri et*

al. [2001a] analyzed fluid-mineral inclusions, interpreted as fluids produced by closed-system antigorite breakdown, in Almirez chl-harzburgite olivines. They reported inclusion trace element patterns showing no depletion of HFSE relative to LILE suggesting that HFSE were mobilized in deserpentinization fluids. However, in a recent improved LA-ICP-MS data set of fluid inclusions in the same Almirez samples, *Scambelluri et al.* [2004a] have shown, in good agreement with our results, that such fluids show trace element patterns that are indeed strongly depleted in Nb relative to LILE and some LREE [*Scambelluri et al.*, 2004a, Table 2 and Figure 6a]. Future improvement of the precision of the absolute trace element concentrations of fluid inclusions will be useful to understand their relationships with the elemental fractionation observed in Almirez atg-serpentinite and chl-harzburgite whole rocks.

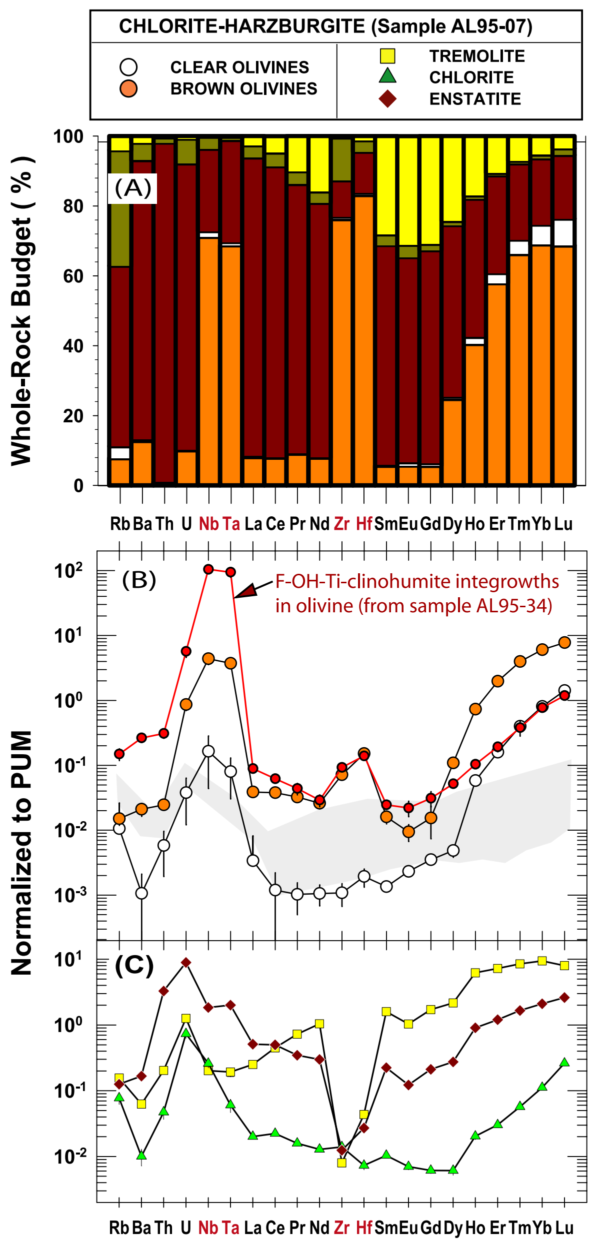

Figure 3. (a) Cumulative percentage bar diagram showing the relative contribution to the whole rock budget of the different constituting minerals in Almirez chlorite-harzburgite sample AL95-07. We have calculated the relative contributions of each mineral by mass balance computations combining the modal percentage abundance of each mineral, whole rock analyses by ICP-MS (Table 1), and trace element analyses by LA-ICP-MS (Table 2) of mineral from this sample. Trace element budgets are recast to 100%. (b and c) In situ trace element abundances analyzed by LA-ICP-MS of harzburgite minerals normalized to the primitive upper mantle [*Sun and McDonough*, 1989]. Trace elements are arranged in order of decreasing incompatibility in a melt/peridotite system. All mineral trace element patterns are the average of *n* analyses of a given mineral in chlorite-harzburgite sample AL95-07 (see also Table 2), except the pattern of F-OH-Ti clinohumite that corresponds to the average of analyses of F-OH-Ti-clinohumite-olivine intergrowths (Figure 4) in chlorite-harzburgite AL95-34 (Table 2). The gray field in Figure 3b is the field of trace element patterns observed in mantle olivines from orogenic massifs and xenoliths [*Bedini and Bodinier*, 1999; *Garrido et al.*, 2000; *Sun and Kerrich*, 1995].

6. Implications for Subduction-Related Magmatism

[12] Prograde chl-harzburgite is expected to occur in subduction zones due to high-pressure dehydration of atg-serpentinite (Field 1 in Figure 6a; Figure 6b) generated by hydration of peridotites from the mantle wedge and the slab [*Hacker et al.*, 2003b; *Rüpke et al.*, 2004; *Schmidt and Poli*, 1998; *Ulmer and Trommsdorff*, 1995]. “Slab serpentinites” are produced by subduction of transform-faults and oceanic lithosphere formed at slow-spreading ridges [*Mével*, 2003, and references therein]. Steady inputs of slab serpentinite may be caused by serpentinization of slab peridotites in the trench-outer rise region of subduction zones by pervasive infiltration of seawater into the bent slab [*Peacock*, 2001; *Ranero et al.*, 2003]. Dehydration of slab serpentinites is the most likely origin of the lower plane of double seismic zone observed in some subduction zones [*Hyndman and Peacock*, 2003; *Peacock*, 2001; *Yamasaki and Seno*, 2003]. There is also wide geological and geophysical

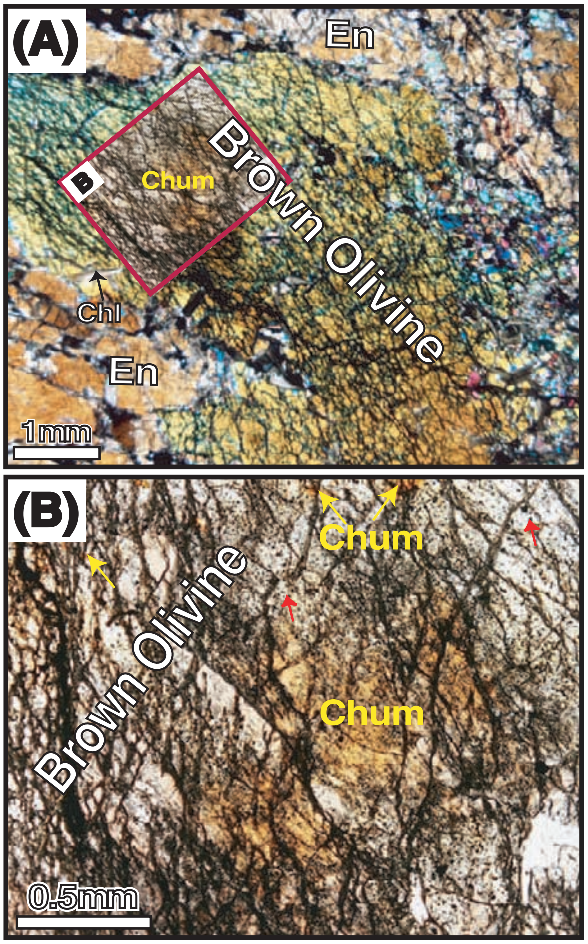

Figure 4. Petrographic evidence for the existence of F-Ti-OH-clinohumite intergrowths in chlorite-harzburgite olivine from the Almirez ultramafic massif. (a) Micrograph (cross-polarized light) of chlorite-harzburgite sample AL95-34 showing coarse-grained brown olivine and enstatite (En) in a matrix of granoblastic enstatite and olivine, and flaky chlorite (Chl). In addition to solid inclusions of ilmenite and magnetite (black grains in Figure 4b), brown olivine contains intergrowths of F-OH-Ti-clinohumite. The red inset shows part of the brown olivine under plane-polarized light wherein F-OH-Ti-clinohumite is clearly identified by its characteristic orange color. (b) Enlarged view of the F-OH-Ti-clinohumite intergrowths (plane-polarized light image) within brown olivine (same area as red inset in Figure 4a), showing the transition of F-OH-Ti-clinohumite patches (Chum and yellow arrows) to brown olivine with ilmenite inclusions (opaques; red arrows).

evidence indicating that wedge serpentinite is widespread in subduction zones. Wedge serpentinites are produced by hydration of the fore-arc mantle linked to the free and bound water released by continuous dehydration reactions from subducted slab sediments and basalts (Figure 6b) [*Hyndman and Peacock*, 2003, and references therein].

[13] Experimental [*Iizuka and Nakamura*, 1995; *Trommsdorff et al.*, 2001; *Ulmer and Trommsdorff*, 1999; *Weiss*, 1997; *Wirth et al.*, 2001] and field evidence [e.g., *Scambelluri et al.*, 1995, 2001b; *Yang*, 2003; *Yang and Jahn*, 2000] indicate that clinohumite-bearing assemblages coexists at high-pressure conditions relevant for subduction processes. Ti-clinohumite is stable at P-T conditions of high-pressure atg-serpentinite dehydration reaction and beyond, and may coexist with chl-harzburgite assemblages (Figure 6a, subfield 2a) [*Iizuka and Nakamura*, 1995; *Stalder and Ulmer*, 2001; *Ulmer and Trommsdorff*, 1999; *Weiss*,

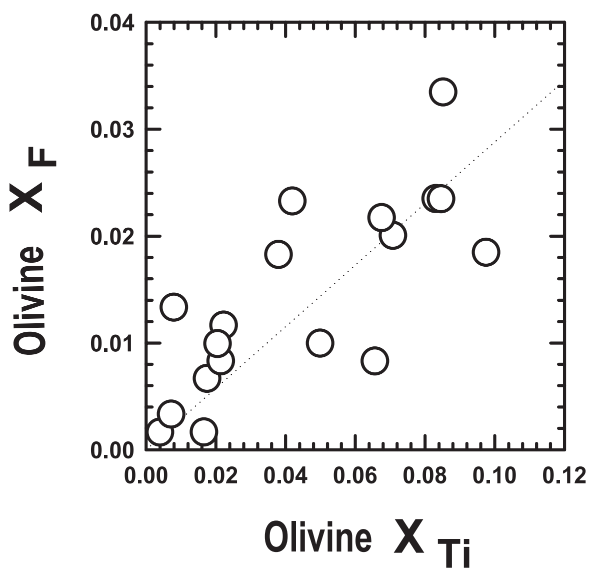

Figure 5. Plot of X_F versus X_{Ti} in olivine-clinohumite intergrowths. X_F is the ratio F/(F + OH) or $^1/_2$ number of F atoms per formula unit of F-OH-Ti clinohumite. X_{Ti} is the number of Ti atoms per formula unit of F-OH-Ti clinohumite. F-OH-Ti-clinohumite formula unit is computed on a 13-cation basis. The observed variation corresponds to 25 mol% of F-OH-Ti-clinohumite intergrowths in the precursor high-Ti "olivine". We have estimated this proportion assuming that Ti and F in olivine are totally hosted in F-OH-Ti-clinohumite intergrowths [*Evans and Trommsdorff*, 1983]. Mineral analyses were obtained with a Cameca SX50 electron microprobe at the Centro de Instrumentación Científica of the Universidad de Granada (Granada, Spain) using PCO and PET crystals for F and Ti analyses, respectively. Natural fluorite and synthetic $MnTiO_3$ were used as standards for F and Ti, respectively. Analytical conditions were an accelerating voltage of 20 kV, beam current of 20 nA, beam diameter of 5–6 μm, and a peak counting time of 20 s for F and Ti.

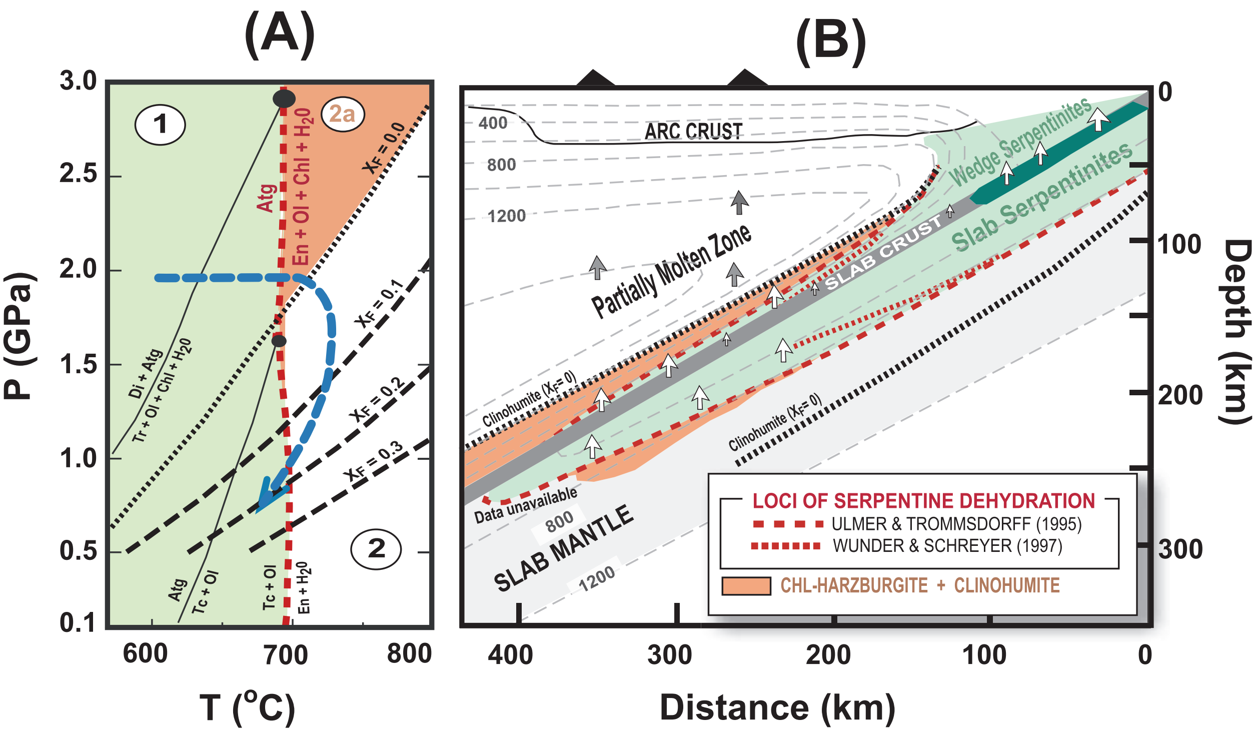

Figure 6. (a) Phase diagram showing some relevant reactions in water-saturated peridotite systems. Field 1 (light green) is the P-T stability field of antigorite. The antigorite-breakdown reaction (dashed, red line) is drawn after experimental data of *Ulmer and Trommsdorff* [1995, 1999]. Other reactions (solid black line) in the antigorite stability field are after *López Sánchez-Vizcaíno et al.* [2001]. Field 2 shows the P-T stability filed of chl-harzburgite. The dotted black line is the clinohumite breakdown reaction (clinohumite = olivine + ilmenite + H_2O) determined experimentally by *Weiss* [1997] for clinohumite with $X_F = 0$, $X_{Fe} = 0.19$, and $X_{Ti} = 0.46$. Subfield 2a (orange) is the P-T range for which chl-harzburgite olivine coexists with this clinohumite composition. Dashed black lines show the effect of variable X_F in the stability of clinohumite [*Trommsdorff et al.*, 2001]. The blue dashed line is the P-T-t metamorphic path deduced for Cerro del Almirez chl-harzburgite [*López Sánchez-Vizcaíno et al.*, 2001]. (b) Thermal model of a cross section of a hydrated, intermediate subduction zone (thermal model for NE Japan after Figure 5c of *Yamasaki and Seno* [2003]). Red lines show the dehydration loci of atg-serpentinite after *Ulmer and Trommsdorff* [1995] (dashed red line) and *Wunder and Schreyer* [1997] (dotted red line). The dotted black lines show the experimentally determined [*Weiss*, 1997] loci of clinohumite ($X_F = 0$) stability (see Figure 6a). For a given pressure, higher fluorine content expands the stability of clinohumite to higher temperatures. The orange area shows the region where olivine and clinohumite are stable in chl-harzburgites for this thermal model (see Figure 6a). Note that in the thermal model the stability field of Ti-clinohumite is represented beyond the P-T conditions shown in Figure 6a, using the experimental data of *Weiss* [1997] at higher P and T. The dark green rectangle in the crust of the incoming slab shows the depth range of the dehydration loci of amphibolite oceanic crust. For amphibolite dehydration, the model uses as an approximate limit of substantial crustal dehydration [*Yamasaki and Seno*, 2003] the boundary between blueschists and lawsonite-eclogites, represented by the reaction glaucophane+clinozoisite = garnet + omphacite + H_2O, releasing about 3 wt% H_2O [*Liu et al.*, 1996].

1997; *Wirth et al.*, 2001]. As a result, clinohumite-olivine intergrowths as those observed in Almirez may be formed in chl-harzburgite at subarc depths both in the mantle wedge and in the subducted slab mantle (Figure 6b). Growth of new prograde olivine after antigorite, together with pervasive presence of fluids, is likely a kinetically favorable scenario for stabilization of humite intergrowths in olivine during deserpentinization. *Wirth et al.* [2001] show that reaction of olivine with TiO_2 and water led to the formation of Ti-clinohumite patches and lamellae within olivine at mantle temperature of 1300 K and depths exceeding 250 km. Some authors have suggested that the stability of F-OH-Ti-clinohumite depends on its fluorine content [*Ulmer and Trommsdorff*, 1999; *Weiss*, 1997]. For a given pressure, increasing fluorine content expands the stability of clinohumite to higher temperatures (Figure 6a) [*Trommsdorff et al.*, 2001; *Ulmer* *and Trommsdorff*, 1999; *Weiss*, 1997; *Wirth et al.*, 2001]. This is the case with Almirez chl-harzburgite where prograde chl-harzburgite olivine coexists with F-OH-Ti-clinohumite at lower pressures due to its higher fluorine content (X_F = 0.1) (Figure 6a).

[14] As the role of serpentinite as a fertile source of H_2O-rich fluids in arcs, the relevance of clinohumite-olivine intergrowths for arc processes relies on the thermal state and history of the subduction zone, as well as the extent of hydration of wedge and slab peridotites [*Hacker et al.*, 2003b; *Peacock*, 2003; *Rüpke et al.*, 2004; *Schmidt and Poli*, 1998]. Following *Schmidt and Poli*'s [1998] terminology, only in hydrated intermediate to warm subduction zones, the breakdown of atg-serpentine would be an adequate source of fluids at subarc depth relevant for arc volcanism genesis. The generality of the latter statement is unavoidably model dependent, however, and it relies on such unknown model parameters as the rheology of the hydrated subarc mantle [*Kelemen et al.*, 2003b, and references therein]. Mapping of relevant deserpentinization and clinohumite equilibria using, for instance, a conventional thermal model of an intermediate subduction zone such as NE Japan [*Yamasaki and Seno*, 2003] indicates that prograde chl-harzburgite olivine may coexist with clinohumite at pertinent subarc depths both in the slab mantle and the mantle wedge (Figure 6b). In such settings, the crustal slab would be sandwiched between mantle slab and wedge regions where olivine and Ti-clinohumite coexist in a fluid-saturated environment (Figure 6b). Other experimental estimates of the antigorite dehydration reaction [*Wunder and Schreyer*, 1997] would not modify this scenario (Figure 6b). Chl-harzburgite may be also stable in other subduction environments, although not necessarily at depths relevant for arc petrogenesis [e.g., *Hacker et al.*, 2003a].

[15] The geochemical relevance of the Almirez chl-harzburgites for subduction processes hinges on their potential to coevally retain HFSE and release fluid at subarc depth. The field-based and geochemical evidence provided by our study fits with a multisource, hybrid "slab-wedge" origin for the HFSE depletion in subduction fluids [*Walker et al.*, 2001]. HFSE retention in chl-harzburgites is achieved by the stabilization of F-OH-Ti-clinohumite intergrowths in chl-harzburgite olivine. As shown in Figure 6 and discussed above, the stabilization of F-OH-Ti-clinohumite intergrowths in chl-harzburgite occurs in both the slab and wedge mantle. Mere closed-system dehydration of slab serpentinite is unlikely to generate the HFSE over enrichments observed in Almirez chl-harzburgites, however (Figure 2a). Slab deserpentinization may likely contribute but not account entirely for the HFSE depletion characterizing subduction fluids. Our data also show that LILE, Pb and Sr behave as immobile elements during the formation of chl-harzburgite. Therefore high LILE/LREE, Pb/Ce and Sr/Nd ratios commonly observed in arc basalts must be imposed by crustal slab lithologies [e.g., *Plank and Langmuir*, 1998]. In that respect, slab deserpentinization may simply act as a fertile source of H_2O-rich fluids that selectively leaches out LILE, Pb and Sr from the overlying crust and sediments on their way up to the mantle wedge (Figure 6b). Overlying wedge chl-harzburgites, on the other hand, may act as HFSE filters efficiently scavenging these elements from the fluids emanating from the slab without modifying their Pb, Sr or LILE content. As fluorine expands the stability field of clinohumite [*Weiss*, 1997] (Figure 6a) and increases the solubility of HFSE in fluids [*Keppler*, 1996], the role of wedge chl-harzburgites in retaining HFSE would be enhanced in settings where slab fluids are fluorine-rich. Resulting fluids in equilibrium with wedge chl-harzburgite would be hence drastically depleted in HFSE and transfer this depletion to the hotter upper levels of the mantle wedge where subduction magmas are generated (Figure 6b). In hydrated subduction settings, stabilization of clinohumite intergrowths in chl-harzburgite olivine may thus play a dualistic role in generating HFSE depletion in subduction fluids by preferentially partitioning HFSE into dehydration residues during slab deserpentinization, and, more importantly, into wedge chl-harzburgites that scavenge HFSE from fluids emanating from the slab (Figure 6b). Our results add weight to increasing evidence for the importance of deserpentinization reactions and their products as sources and sinks for H_2O, Cl, F, B, Li and Be at subarc depths in the genesis of subduction-related magmatism [*Scambelluri et al.*, 2004b; *Scambelluri and Philippot*, 2001; *Straub and Layne*, 2003a, 2003b].

Acknowledgments

[16] Tim Elliot and two anonymous reviewers are thanked for insightful and helpful reviews. We are also grateful to Terry

Plank, Peter Ulmer, and Marco Scambelluri for constructive criticism on previous versions of this manuscript. N. W. Rogers (Open University) and S. Pourtales (Université de Montpellier 2) are acknowledged for facilitating access to the Open University LA-ICP-MS and assistance during ICP-MS analyses at ISTEEM, respectively. This work is supported by the Spanish ''Ministerio de Educación y Ciencia'' through a ''Ramón y Cajal'' fellowship to C.J.G. and research grant BTE 2004-1489 to M.T.G.M., and the ''Junta de Andalucía'' research groups RNM-0145 and RNM-0131. This research has been partly funded by the European Funds for Regional Development (FEDER).

References

Alard, O., J. M. Dautria, and J. L. Bodinier (1996), Nature of the upper mantle and metasomatic processes on either side of the Sillon Houiller (French Massif central), *C. R. Acad. Sci. Ser IIa Sci. Terre Planetes*, *323*(9), 763–770.

Bedini, R. M., and J. L. Bodinier (1999), Distribution of incompatible trace elements between the constituents of spinel peridotite xenoliths: ICP-MS data from the East African Rift, *Geochim. Cosmochim. Acta*, *63*(22), 3883–3900.

Bodinier, J. L., and M. Godard (2003), Orogenic, ophiolitic, and abyssal peridotites, in *Treatise on Geochemistry*, vol. 2, *Geochemistry of the Mantle and Core*, edited by R. W. Carlson, Elsevier, New York.

Downes, H., M. K. Reichow, P. R. D. Mason, A. D. Beard, and M. F. Thirlwall (2003), Mantle domains in the lithosphere beneath the French Massif Central: Trace element and isotopic evidence from mantle clinopyroxenes, *Chem. Geol.*, *200*(1–2), 71–87.

Evans, B. W., and V. Trommsdorff (1983), Fluorine hydroxyl titanian clinohumite in Alpine recrystallized garnet peridotite: Compositional controls and petrologic significance, *Am. J. Sci.*, *283A*, 355–369.

Garrido, C. J., J. L. Bodinier, and O. Alard (2000), Incompatible trace element partitioning and residence in anhydrous spinel peridotites and websterites from the Ronda orogenic peridotite, *Earth Planet. Sci. Lett.*, *181*(3), 341–358.

Godard, M., D. Jousselin, and J. L. Bodinier (2000), Relationships between geochemistry and structure beneath a palaeo-spreading centre: A study of the mantle section in the Oman ophiolite, *Earth Planet. Sci. Lett.*, *180*(1–2), 133–148.

Gómez-Pugnaire, M. T., P. Ulmer, and V. López Sánchez-Vizcaíno (2000), Petrogenesis of the mafic igneous rocks of the Betic Cordilleras: A field, petrological and geochemical study, *Contrib. Mineral. Petrol.*, *139*(4), 436–457.

Govindaraju, K. (1994), Compilation of working values and sample description for 383 geostandards, *Geostand. Newsl.*, *XVIII*(Spec. Issue), 1–158.

Hacker, B. R., G. A. Abers, and S. M. Peacock (2003a), Subduction factory 1. Theoretical mineralogy, densities, seismic wave speeds, and H^2O contents, *J. Geophys. Res.*, *108*(B1), 2029, doi:10.1029/2001JB001127.

Hacker, B. R., S. M. Peacock, G. A. Abers, and S. D. Holloway (2003b), Subduction factory 2. Are intermediate-depth earthquakes in subducting slabs linked to metamorphic dehydration reactions?, *J. Geophys. Res.*, *108*(B1), 2030, doi:10.1029/2001JB001129.

Hürlimann, R. (1999), Die Hochdruckmetamorphose der Ultramafika und der angrenzenden Nebengesteine am Cerro de Almirez, Sierra Nevada, Südspanien (Teil II), thesis, 105 pp., ETH, Zurich.

Hyndman, R. D., and S. M. Peacock (2003), Serpentinization of the forearc mantle, *Earth Planet. Sci. Lett.*, *212*(3–4), 417–432.

Iizuka, Y., and E. Nakamura (1995), Experimental study of the slab–mantle interaction and implications for the formation of titanoclinohumite at deep subduction zone, *Proc. Jpn. Acad.*, *71*, 159–164.

Ionov, D. A., L. Savoyant, and C. Dupuy (1992), Application of the ICP-MS technique to trace-element analysis of peridotites and their minerals, *Geostand. Newsl.*, *16*(2), 311–315.

Jochum, K. P., H. M. Seufert, and M. F. Thirwall (1990), Multi-element analysis of 15 international standard rocks by isotope-dilution spark source mass spectrometry (ID-SSMS), *Anal. Chem.*, *331*, 104–110.

Jochum, K. P., et al. (2000), The preparation and preliminary characterisation of eight geological MPI-DING reference glasses for in-situ microanalysis, *Geostand. Newsl.*, *24*(1), 87–133.

Kelemen, P. B., K. T. M. Johnson, R. J. Kinzler, and A. J. Irving (1990), HFSE depletions in arc basalts due to mantle magma interaction, *Nature*, *345*(6275), 521–524.

Kelemen, P. B., K. Hanghøj, and A. R. Greene (2003a), One view of the geochemistry of subduction-related magmatic arcs, with emphasis on primitive andesite and lower crust, in *Treatise on Geochemistry*, vol. 3, *Geochemistry of the Crust*, edited by R. Rudnick, Elsevier, New York.

Kelemen, P. B., J. L. Rilling, E. M. Parmentier, L. Mehl, and B. R. Hacker (2003b), Thermal structure due to solid-state flow in the mantle wedge beneath arcs, in *Inside the Subduction Factory*, *Geophys. Monogr. Ser.*, vol. 138, edited by J. M. Eiler, pp. 293–311, AGU, Washington, D. C.

Keppler, H. (1996), Constraints from partitioning experiments on the composition of subduction-zone fluids, *Nature*, *380*(6571), 237–240.

Kitamura, K., S. Kondoh, N. Morimoto, G. H. Miller, G. R. Rossman, and A. Putnis (1987), Planar OH-bearing defects in mantle olivine, *Nature*, *328*, 143–145.

Liu, J., S. R. Bohlen, and W. G. Ernst (1996), Stability of hydrous phases in subducting oceanic crust, *Earth Planet. Sci. Lett.*, *143*(1–4), 161–171.

Longerich, H. P., S. E. Jackson, and D. Günther (1996), Laser ablation inductively coupled plasma mass spectrometric transient signal data acquisition and analyte concentration calculation, *J. Anal. At. Spectrosc.*, *11*, 899–904.

López Sánchez-Vizcaíno, V., D. Rubatto, M. T. Gómez-Pugnaire, V. Trommsdorff, and O. Müntener (2001), Middle Miocene high-pressure metamorphism and fast exhumation of the Nevado-Filabride Complex, SE Spain, *Terra Nova*, *13*(5), 327–332.

Mével, C. (2003), Serpentinization of abyssal peridotites at mid-ocean ridges, *C. R. Acad. Sci. Ser IIa Sci. Terre Planetes*, *335*(10–11), 825–852.

Peacock, S. M. (2001), Are the lower planes of double seismic zones caused by serpentine dehydration in subducting oceanic mantle?, *Geology*, *29*(4), 299–302.

Peacock, S. M. (2003), Thermal structure and metamorphic evolution of subducting slabs, in *Inside the Subduction Factory*, *Geophys. Monogr. Ser.*, vol. 138, edited by J. M. Eiler, AGU, Washington, D. C.

Pearce, N. J. G., W. T. Perkins, J. A. Westgate, M. P. Gorton, S. E. Jackson, C. R. Neal, and S. P. Chenery (1997), A compilation of new and published major and trace element data for NIST SRM 610 and NIST SRM 612 glass reference materials, *Geostand. Newsl.*, *21*(1), 115–144.

Plank, T., and C. H. Langmuir (1998), The chemical composition of subducting sediment and its consequences for the crust and mantle, *Chem. Geol.*, *145*(3–4), 325–394.
Puga, E., J. M. Nieto, A. Díaz de Federico, J. L. Bodinier, and L. Morten (1999), Petrology and metamorphic evolution of ultramafic rocks and dolerite dykes of the Betic Ophiolitic Association (Mulhacen Complex, SE Spain): Evidence of eo-Alpine subduction following an ocean-floor metasomatic process, *Lithos*, *49*(1–4), 23–56.
Ranero, C. R., J. Phipps Morgan, K. McIntosh, and C. Reichert (2003), Bending-related faulting and mantle serpentinization at the Middle America trench, *Nature*, *425*(6956), 367–373.
Risold, A. C., V. Trommsdorff, and B. Grobéty (2001), Genesis of ilmenite rods and palisades along humite-type defects in olivine from Alpe Arami, *Contr. Mineral. Petrol.*, *140*, 619–628.
Ruiz Cruz, M. D., E. Puga, and J. M. Nieto (1999), Silicate and oxide exsolution in pseudo-spinifex olivine from metaultramafic rocks of the Betic Ophiolitic Association: A TEM study, *Am. Miner.*, *84*(11–12), 1915–1924.
Rüpke, L. H., J. Phipps Morgan, M. Hort, and J. A. D. Connolly (2004), Serpentine and the subduction zone water cycle, *Earth Planet. Sci. Lett.*, *223*(1–2), 17–34.
Scambelluri, M., and P. Philippot (2001), Deep fluids in subduction zones, *Lithos*, *55*(1–4), 213–227.
Scambelluri, M., O. Müntener, J. Hermann, G. B. Piccardo, and V. Trommsdorff (1995), Subduction of water into the mantle—History of an alpine peridotite, *Geology*, *23*(5), 459–462.
Scambelluri, M., G. B. Piccardo, P. Philippot, A. Robbiano, and L. Negretti (1997), High salinity fluid inclusions formed from recycled seawater in deeply subducted alpine serpentinite, *Earth Planet. Sci. Lett.*, *148*(3–4), 485–499.
Scambelluri, M., P. Bottazzi, V. Trommsdorff, R. Vannucci, J. Hermann, M. T. Gomez-Pugnaire, and V. López Sánchez-Vizcaíno (2001a), Incompatible element-rich fluids released by antigorite breakdown in deeply subducted mantle, *Earth Planet. Sci. Lett.*, *192*(3), 457–470.
Scambelluri, M., E. Rampone, and G. B. Piccardo (2001b), Fluid and element cycling in subducted serpentinite: A trace-element study of the Erro-Tobbio high-pressure ultramafites (Western Alps, NW Italy), *J. Petrol.*, *42*(1), 55–67.
Scambelluri, M., J. Fiebig, N. Malaspina, O. Müntener, and T. Pettke (2004a), Serpentinite subduction: Implications for fluid processes and trace-element recycling, *Int. Geol. Rev.*, *46*(7), 595–613.
Scambelluri, M., O. Müntener, L. Ottolini, T. T. Pettke, and R. Vannucci (2004b), The fate of B, Cl and Li in the subducted oceanic mantle and in the antigorite breakdown fluids, *Earth Planet. Sci. Lett.*, *222*(1), 217–234.
Schmidt, M. W., and S. Poli (1998), Experimentally based water budgets for dehydrating slabs and consequences for arc magma generation, *Earth Planet. Sci. Lett.*, *163*(1–4), 361–379.
Schönbächler, M. (1999), Die Hochdruckmetamorphose der Ultramafika und der angrenzenden Nebengesteine am Cerro de Almirez, Sierra Nevada, Südspanien (Teil I), thesis, ETH, Zurich.
Stalder, R., and P. Ulmer (2001), Phase relations of a serpentine composition between 5 and 14 GPa: Significance of clinohumite and phase E as water carriers into the transition zone, *Contrib. Mineral. Petrol.*, *140*(6), 670–679.
Straub, S. M., and G. D. Layne (2003a), Decoupling of fluids and fluid-mobile elements during shallow subduction: Evidence from halogen-rich andesite melt inclusions from the Izu arc volcanic front, *Geochem. Geophys. Geosyst.*, *4*(7), 9004, doi:10.1029/2002GC000349.
Straub, S. M., and G. D. Layne (2003b), The systematics of chlorine, fluorine, and water in Izu arc front volcanic rocks: Implications for volatile recycling in subduction zones, *Geochim. Cosmochim. Acta*, *67*(21), 4179–4203.
Sun, M., and R. Kerrich (1995), Rare earth element and high field strength element characteristics of whole rocks and mineral separates of ultramafic nodules in Cenozoic volcanic vents of southeastern British Columbia, Canada, *Geochim. Cosmochim. Acta*, *59*(23), 4863–4879.
Sun, S.-S., and W. F. McDonough (1989), Chemical and isotopic systematics of oceanic basalts: Implications for mantle composition and processes, in *Magmatism in the Ocean Basins*, edited by A. D. Saunders and M. J. Norry, *Geol. Soc. Spec. Publ.*, *42*, 313–345.
Tatsumi, Y., and S. Eggins (1995), *Subduction Zone Magmatism*, 211 pp., Blackwell Sci., Malden, Mass.
Tatsumi, Y., D. L. Hamilton, and R. W. Nesbitt (1986), Chemical characteristics of fluid phase released from a subducted lithosphere and origin of arc magmas—Evidence from high-pressure experiments and natural rocks, *J. Volcanol. Geotherm. Res.*, *29*(1–4), 293–309.
Thompson, J. B. J. (1978), Biopyroboles and polysomatic series, *Am. Mineral.*, *63*, 239–249.
Tilley, C. E. (1951), The zoned contact-skarns of the Broadford area, Skye: A study of boron-fluorine metasomatism in dolomites, *Mineral. Mag.*, *29*(621).
Trommsdorff, V., and B. W. Evans (1980), Titanian hydroxylclinohumite—Formation and breakdown in antigorite rocks (Malenco, Italy), *Contrib. Mineral. Petrol.*, *72*(3), 229–242.
Trommsdorff, V., V. López Sánchez-Vizcaíno, M. T. Gómez-Pugnaire, and O. Muentener (1998), High pressure break-down of antigorite to spinifex-textured olivine and orthopyroxene, SE Spain, *Contrib. Min. Petrol.*, *132*, 139–148.
Trommsdorff, V., A. C. Risold, E. Reusser, J. A. Connolly, and P. Ulmer (2001), Titanian clinohumite: Ilmenite rod inclusions and phase relations (abstract), Central Alps, paper presented at Workshop on Fluid/Slab/Mantle Interactions and UHP Minerals, Waseda University, Tokyo.
Ulmer, P., and V. Trommsdorff (1995), Serpentine stability to mantle depths and subduction-related magmatism, *Science*, *268*(5212), 858–861.
Ulmer, P., and V. Trommsdorff (1999), Phase relations of hydrous mantle subducting to 300 km, in *Mantle Petrology: Field Observations and High-Pressure Experimentation*, edited by Y. Fei, C. M. Bertka, and B. O. Mysen, pp. 259–281, Geochem. Soc., Houston, Tex.
Van Achtebergh, E., C. G. Ryan, S. E. Jackson, and W. L. Griffin (2001), Data reduction software for LA-ICP-MS, in *Laser-Ablation-ICPMS in the Earth Sciences: Principles and Applications*, edited by P. J. Sylvester, pp. 239–243, Mineral. Assoc. of Can., Ottawa, Ontario, Canada.
Veblen, D. R. (1991), Polysomatism and polysomatic series—A review and applications, *Am. Miner.*, *76*(5–6), 801–826.
Walker, J. A., L. C. Patino, M. J. Carr, and M. D. Feigenson (2001), Slab control over HFSE depletions in central Nicaragua, *Earth Planet. Sci. Lett.*, *192*(4), 533–543.
Weiss, M. (1997), Clinohumites: A field and experimental study, Ph.D. thesis, ETH, Zurich.
Wirth, R., L. F. Dobrzhinetskaya, and H. W. Green (2001), Electron microscope study of the reaction olivine plus $H_2O + TiO_2$ = titanian-clinohumite plus titanian-chondrodite

synthesized at 8 GPa, 1300 K, *Am. Miner.*, *86*(5–6), 601–610.

Wunder, B., and W. Schreyer (1997), Antigorite: High-pressure stability in the system MgO-SiO_2–H_2O (MSH), *Lithos*, *41*(1–3), 213–227.

Yamasaki, T., and T. Seno (2003), Double seismic zone and dehydration embrittlement of the subducting slab, *J. Geophys. Res.*, *108*(B4), 2212, doi:10.1029/2002JB001918.

Yang, J. J. (2003), Titanian clinohumite-gamet-pyroxene rock from the Su-Lu UHP metamorphic terrane, China: Chemical evolution and tectonic implications, *Lithos*, *70*(3–4), 359–379.

Yang, J. J., and B. M. Jahn (2000), Deep subduction of mantle-derived garnet peridotites from the Su-Lu UHP metamorphic terrane in China, *J. Metamorph. Geol.*, *18*(2), 167–180.